Computational investigation of porous media phase field formulations: microscopic, effective macroscopic, and Langevin equations

Antonis Veveris, Markus Schmuck

Computational investigation of porous media phase field formulations: microscopic, effective macroscopic, and Langevin equations

Antonis Veveris and Markus Schmuck[1]

Maxwell Institute for Mathematical Sciences and
School for Mathematical and Computer Sciences
Heriot-Watt University
Edinburgh, EH144AS

Abstract

We consider upscaled/homogenized Cahn-Hilliard/Ginzburg-Landau phase field equations as mesoscopic formulations for interfacial dynamics in strongly heterogeneous domains such as porous media. A recently derived effective macroscopic formulation, which takes systematically the pore geometry into account, is computationally validated. To this end, we compare numerical solutions obtained by fully resolving the microscopic pore-scale with solutions of the upscaled/homogenized porous media formulation. The theoretically derived convergence rate $\mathcal{O}(\epsilon^{1/4})$ is confirmed for circular pore-walls. An even better convergence of order $\mathcal{O}(\epsilon^1)$ holds for square shaped pore-walls. We also compute the homogenization error over time for different pore geometries. We find that the quality of the time evolution shows a complex interplay between pore geometry and heterogeneity. Finally, we study the coarsening of interfaces in porous media with computations of the homogenized equation and the microscopic formulation fully resolving the pore space. We recover the experimentally validated and theoretically rigorously derived coarsening rate of $\mathcal{O}(t^{1/3})$ in the periodic porous media setting. In the case of *critical quenching* and after adding thermal noise to the microscopic porous media formulation, we observe that the influence of thermal fluctuations on the coarsening rate shows after a short, expected phase of universal coarsening, a sharp transition towards a different regime.

Keywords: complex heterogeneous systems, phase transition, homogenization, upscaling, coarsening, criticality, universality, porous media, finite elements,
2010 MSC: 00-01, 99-00

1. Introduction

Over the last decades, phase field modelling has received increasing interest for theoretical and computational investigation of physical, chemical and even experimental systems inspired by the work of Cahn and Hilliard [1]. However, the idea of diffuse interface modelling seems to go back to van der Waals [2]. The variational structure based on free energies allows for thermodynamic modelling of phase transitions [3, 4] and it serves as a predictive tool in engineering of fluid mechanics [5], multiphase flow [6, 7, 8], fuel cells [9, 10], batteries [11], and porous media [12]. Since many systems and applications involve strongly heterogeneous media, we refer to these by the general term Complex Heterogeneous Multiphase Systems. From a numerical point of view, strong heterogeneities lead to computationally high dimensional systems since the mesh size $h > 0$ has to be chosen much smaller than the heterogeneity $\epsilon > 0$, i.e., $0 < h \ll \epsilon$. The heterogeneity parameter is defined by $\epsilon = \frac{\ell}{\Lambda}$ where ℓ denotes a material specific microscale, e.g., characteristic pore size, and Λ is the macroscopic size of the porous medium. As a consequence, an effective macroscopic phase field equation has been derived in [13, 14] that does not depend on such a restricting mesh constraint. In fact, a first attempt of extending the framework towards fluid flow is [15] albeit requiring specific assumptions such

[1]Corresponding author. http://www.macs.hw.ac.uk/ ms713/

as flows with large Péclet number. Recently, diffuse interface formulations are gaining increasing interest in studying contact lines and droplets on solid substrates [16, 17, 18, 19]. Phase field formulations provide also a convenient computational alternative to sharp interface models. It has been applied in modelling dynamics of multicomponent vesicles [20] or as a computational tool for bubble dynamics [21]. In [22] the authors study the problem of surface diffusion based on a diffuse interface formulation and similarly in [23], the authors look at the problem of phase transition and coarsening on surfaces. Similarly, coarsening is considered for an interacting particle system in [24]. Another more recent and promising extension of Cahn and Hilliard's diffuse interface concept is the phase field crystal method [25] which takes atomistic information into account for modelling crystal growth as proposed in [26, 27]. The Ginzburg-Landau functional leads also to a mathematical theory in superconductivity where the study of minimizers and asymptotic limits is equally important, e.g. [28, 29].

In this article, we computationally investigate the models recently derived in [13, 14]. We introduce numerical methods for validating the rigorously derived error estimates from [30] and for studying dynamics of contactlines [16, 18, 31] in porous media. Finally, we validate the well-accepted physical phenomenon of coarsening of phase separating systems in strongly heterogeneous media [32, 33, 34]. It is well-known that late stages of first-order phase transitions in homogeneous domains [32, 35, 36] show a power law growth with exponent 1/3. This universal behaviour has been put on a rigorous basis in [33]. Our computations based on a full microscopic as well as an upscaled/homogenized phase field formulation recover this universal scaling. The structure of the paper is as follows: in the next paragraph we first recall the basic concepts and results of the Ginzburg-Landau/Cahn-Hilliard phase field theory. In Section 2, we introduce the different phase field formulations of interest, i.e., a microscopic, a novel effective macroscopic, and a microscopic description that accounts for thermal fluctuations. We provide numerical discretizations of these models and study convergence in Section 3. The influence of pore geometry/heterogeneities on the coarsening is the topic of Section 4.

Phase field modelling. Phase ordering/transition is generally described by a coarse grained local order parameter $\phi(\mathbf{x},t) : D\times(0,T)\to\mathbb{R}$, on a bounded domain $D\subset\mathbb{R}^d$ where d is the dimension of space and $0<T<\infty$ the maximum time of observation. We choose $D:=[0,1]^2$ to be the unit square for our computations later on. The phase field variable ϕ is phenomenologically characterised by the Ginzburg-Landau/Cahn-Hilliard free energy in absence of external fields, that is,

$$F(\phi)=\frac{1}{|D|}\int_D f(\phi)\,d\mathbf{x}\,, \tag{1}$$

here normalized by by the Lebesgues measure $|D|=1$ of the domain D. The energy density $f(\phi):=f_L(\phi)+\frac{\lambda^2}{2}\left|\nabla\phi\right|^2$ consists of the homogeneous free energy

$$f_L(\phi)=a(\theta)\phi^2+\frac{b}{2}\phi^4\,, \tag{2}$$

with $a(\theta):=a_0(\theta-\theta_c)<0$, θ_c a given critical temperature, and $a_0>0$, and $b>0$. The parameter $\lambda>0$ is proportional to the interfacial width. The gradient term in (1) allows for diffuse interfaces. A dynamic description of ϕ is generally obtained by minimizing (1) over time with the help of a gradient descent/flow, i.e., we are looking for solutions ϕ of

$$(\partial_t\phi,v)=-\frac{\delta^V F(\phi)}{\delta^V\phi}=-\left(\nabla^V_\phi F(\phi),v\right)_V\,,\qquad\text{for all } v\in V\,, \tag{3}$$

where $(\cdot,\cdot):=(\cdot,\cdot)_{L^2}$ denotes the L^2-scalar product if $V=L^2$, and it is the H^1 semi-inner product $(\cdot,\cdot)_V:=(\hat{\mathrm{M}}\nabla\cdot,\nabla\cdot)$ for symmetric, positive definite tensors $\hat{\mathrm{M}}\in\mathbb{R}^{d\times d}$ if $V=H^1$. The Fréchet derivative $\frac{\delta^V F(\phi)}{\delta^V\phi}=\left(\nabla^V_\phi F(\phi),v\right)_V$ allows us to uniquely identify the functional derivative ∇^V_ϕ by Riesz representation theorem

[37, p.163]. The conservation of mass is obtained for $V = H^1$ which leads to the well-known Cahn-Hilliard equation [1], that is,

$$\partial_t \phi = \operatorname{div}\left(\hat{\mathrm{M}}\nabla\left(f_L'(\phi) - \lambda^2\Delta\phi\right)\right) . \tag{4}$$

We note that the $V = L^2$-gradient flow leads to the Allen-Cahn equation, which is not mass conserving in difference to (4). The double-well character of the free energy (1) arises also in the regular solution theory in the form of the Flory-Huggins energy density [38], i.e.,

$$f_L(\phi) = zc_I\phi(1-\phi) + k_B\theta\left(\phi\ln\,\phi - (1-\phi)\ln(1-\phi)\right) , \tag{5}$$

where k_B is the Boltzmann constant, z counts the number of bonds with neighbouring species and is called coordination number, and c_I represents an mean field interaction energy. In this article, we will work with the well accepted double-well potential

$$w(\phi) = a\phi^2(1-\phi)^2 , \qquad a > 0 , \tag{6}$$

which reliably captures the phenomenological nature of the energy densities (5) and (2) but generally shows more stable behaviour in computations.

Coarsening and coarsening rates. The coarsening, e.g. [24, 32, 33], describes the time evolution of a characteristic length $L(t)$ which is defined as

$$L := 1/F(\phi) , \tag{7}$$

where f represents the interfacial area per unit volume(/perimeter per unit volume) and hence L has units of length. We note that Kohn and Otto [33] made a step change in the rigorous understanding by proving the time-averaged coarsening rates

$$\frac{1}{T}\int_0^T F^2\,dt \geq \frac{C}{T}\int_0^T (t^{-1/3})^2\,dt , \qquad \text{for } T \gg 1 . \tag{8}$$

However, the following classical statement

$$L \leq Ct^{1/3} , \tag{9}$$

still lacks a rigorous argument. In Section 4, we will computationally investigate the influence of pore geometries to the coarsening rates computed by the characteristic length L defined in (7).

2. Microscopic, effective macroscopic, and Langevin dynamics of phase field equations

Before we state the different phase field formulations, we introduce necessary notation and definitions. For simplicity, we focus here on periodic porous media which are defined by a reference cell Y which represents a material specific(/statistically averaged) pore geometry Y^1 by removing a material specific solid phase Y^2 such as a spherical, a square-shaped, or an elliptical solid particle, see Fig. 1. In fact, this cell Y can also be a periodic porous medium itself.

The subsequent effective macroscopic phase field formulation also requires the well-accepted thermodynamic concept of Local Thermodynamic Equilibrium (LTE).

Definition 1. (LTE) *The chemical potential μ assocated with the homogeneous phase field free energy density f_L in (1) is $\mu(\phi) = -\lambda\Delta\phi + \frac{1}{\lambda}f_L(\phi)$, and we denote the corresponding upscaled chemical potential by*

$\mu_0(\phi_0) = -\lambda \mathrm{div}(\hat{\mathrm{D}}\nabla\phi_0) + \frac{1}{\lambda} f_L(\phi_0) = \lambda w_0 + \frac{1}{\lambda} f_L(\phi_0)$, *where* $\hat{\mathrm{D}}$ *is the porous media correction tensor (16). We say that* μ_0 *is in* local thermodynamic equilibrium (LTE) *if and only if*

$$\frac{\partial \mu_0(\phi_0(\mathbf{x}))}{\partial x_k} = \begin{cases} 0 & \text{in the cell problem, } D \times Y\,, \\ \frac{\partial \mu_0(\phi_0)}{\partial x_k} & \text{on the macroscale, } D \text{ (after averaging over } Y)\,, \end{cases} \tag{10}$$

where $\phi_0(x)$ *is the upscaled/slow variable, which is independent of the microscale* $\mathbf{y} \in Y$ *and which solves the upscaled phase field equation (15) below.*

Microscopic formulation $(\mathbf{M}^\epsilon)$. We consider phase field equations in perforated domains $D \setminus S^\epsilon =: D^\epsilon \subset \mathbb{R}^d$, $1 \leq d \leq 3$, with characteristic heterogeneity $\epsilon \ll 1$. The pore space D^ϵ and the solid phase S^ϵ are defined with respect to a material specific pore space Y^1, i.e.,

$$D^\epsilon := \bigcup_{\mathbf{z}\in\mathbb{Z}^d} \epsilon\left(Y^1 + \mathbf{z}\right) \cap D\,, \qquad S^\epsilon := \bigcup_{\mathbf{z}\in\mathbb{Z}^d} \epsilon\left(Y^2 + \mathbf{z}\right) \cap D = \Omega \setminus D^\epsilon\,, \tag{11}$$

where the subsets Y^1 and the associated characteristic solid phase $Y^2 = Y \setminus Y^1$ are such that D^ϵ is a connected set. In Fig. 1, examples of different pore spaces are depicted by removing solid obstacles S^ϵ given as circles, squares, or ellipses. The ellipses (Fig. 1, **right**) are not cell-centered and hence induce anisotropic transport. Hence, the phase field equation (4) reads in a perforated space time domain $(D^\epsilon)_T := D^\epsilon \times (0,T)$ with spatial boundary $(\partial D^\epsilon)_T := \partial D^\epsilon \times (0,T)$ and characteristic heterogeneity $\epsilon \ll 1$ as follows

$$(\mathbf{M}^\epsilon) \qquad \begin{cases} \partial_t \phi^\epsilon = \mathrm{div}\left(\hat{\mathrm{M}}\nabla\left(f_L'(\phi^\epsilon) - \lambda^2\Delta\phi^\epsilon\right)\right) & \text{in } (D^\epsilon)_T\,, \\ \mathbf{n}\cdot\nabla\phi^\epsilon = \epsilon A & \text{in } (\partial D^\epsilon)_T\,, \\ \mathbf{n}\cdot\nabla\mu^\epsilon = 0 & \text{in } (\partial D^\epsilon)_T\,, \end{cases} \tag{12}$$

where $\mu = f_L'(\phi^\epsilon) - \lambda^2\Delta\phi^\epsilon$ is the chemical potential associated with $f(\phi)$. The variable $A = -\frac{\gamma}{C_h}\alpha$ accounts for the wetting properties of the pore walls and depends on the Cahn number $C_h = \frac{\lambda}{L}$ and the fraction $\gamma = \frac{2\sqrt{2}\phi_e}{3\sigma_{lg}}$ where ϕ_e is the local equilibrium limiting value of the free energy F and σ_{lg} is the liquid-gas surface tension. For $\alpha > 0$ the pore walls are hydrophilic and for $\alpha < 0$ hydrophobic. Hence, $\alpha = 0$ stands for a contact angle of 90 degrees, i.e., neutral wetting ($A = 0$), which will be the case of interest in this article. Hence, the boundary condition $(12)_3$ imposes impenetrable pore walls (no-flux boundary conditions).

Remark 1. *We note that the wetting boundary condition* $(12)_2$ *is already classical by now and has been widely applied in modelling contact line dynamics, e.g. [13, 39]. This inhomogeneous boundary condition* $(12)_2$ *appears due to a surface energy contribution to the bulk free energy* $F(\phi)$ *in (1), i.e.,*

$$\Gamma(\phi) = \int_{\partial D^\epsilon} \left(\sigma_{sg} + (\sigma_{sl} - \sigma_{sg}) s(\tilde{\phi})\right) do\,, \tag{13}$$

where σ_{sg} *is the solid-gas surface energy and* σ_{sl} *the solid-liquid surface energy. Using Young's law we replace the difference* $(\sigma_{sl} - \sigma_{sg})$ *by* $(\sigma_{sl} - \sigma_{sg}) = \sigma\cos(\theta_e)$*, where* θ_e *is the equilibrium contact angle and* $s(\tilde{\phi})$ *is polynomial such that* $s(1) = 1$ *and* $s(-1) = 0$ *for an order parameter* $\tilde{\phi}$ *with the two equilibrium limiting values* $\tilde{\phi} = 1$ *representing liquid and* $\phi = -1$ *representing gas. The order parameter* ϕ *is related to* $\tilde{\phi}$ *via* $\phi := \frac{\tilde{\phi}+1}{2}$ *for instance. The polynom* $s(x) = 1/4(-x^3 + 3x + 2)$ *satisfies these constraints and is derived based on surface tension and the given free energy density* f *defining (1). Taking the variational derivative of the total free energy* $E(\phi) = F(\phi) + \Gamma(\phi)$ *with respect to* ϕ *leads to a new term in the surface energy originating from the gradient penalty term in* $F(\phi)$*, i.e.,*

$$\delta E(\phi) = \int_{D^\epsilon} \mu\delta\phi\, do + \int_{\partial D^\epsilon} \left(\lambda^2 \mathbf{n}\cdot\nabla\phi - \sigma\cos(\theta_e) g'(\tilde{\phi})\right)\delta\phi\, do\,, \tag{14}$$

where $\mu = f'(\phi) - \lambda^2\Delta\phi$ *is the chemical potential. This motivates the appearance of the non-homogeneous Neumann boundary condition* $(12)_2$*.* $\diamond$

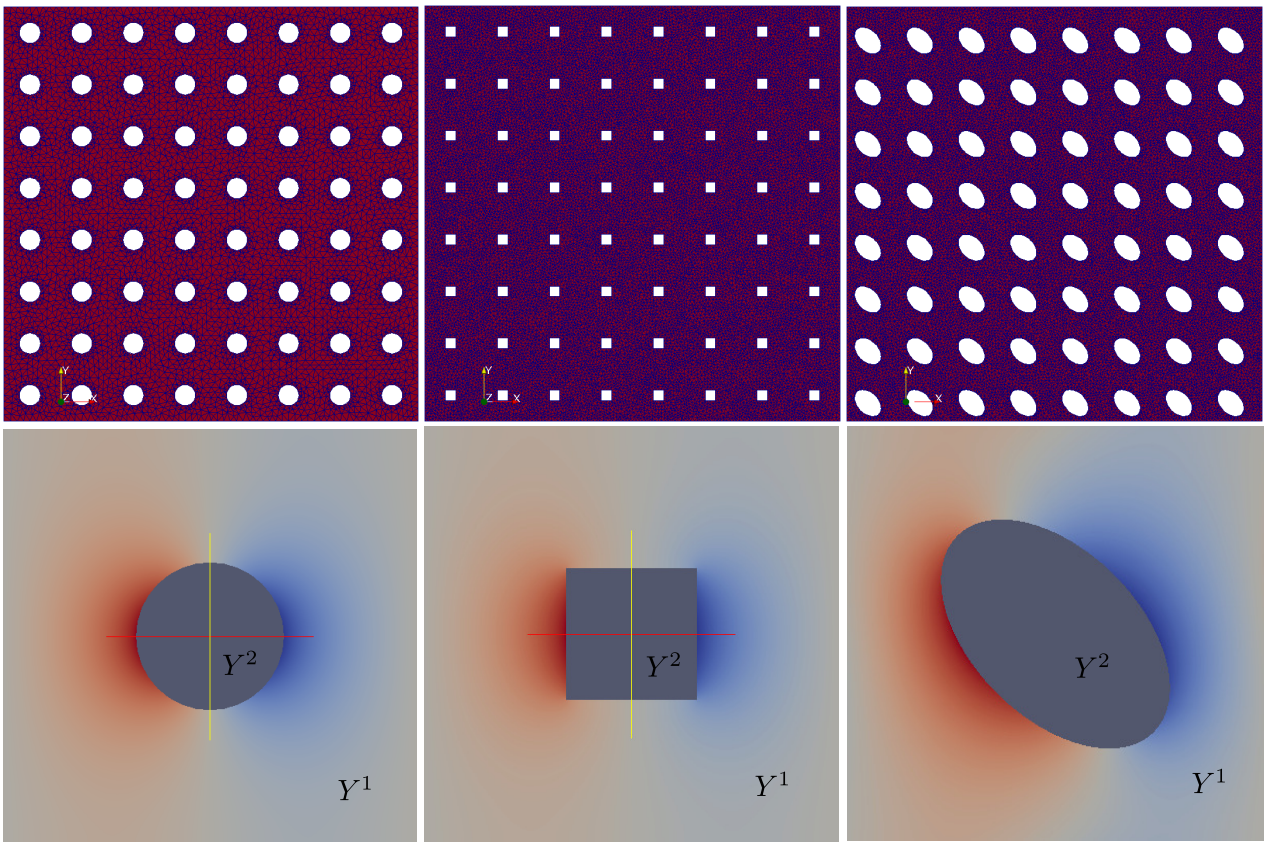

Figure 1: **Top:** Perforated domains D^ϵ with heterogeneity $\epsilon = 0.125$ defined for solid obstacles S^ϵ, i.e., circles **(left)**, squares **(middle)**, and ellipses **(right)**. **Bottom:** Plots (from left to right) for the corrector ξ^1 solving the elliptic reference cell problem (17) for a reference cell Y containing a single circular, square shaped, and elliptical shaped solid obstacle $Y^2 := Y \setminus Y^1$, where Y^1 is the pore space.

Effective macroscopic equations $(\mathbf{M}^0)$. An effective macroscopic phase field formulation for interfacial transport in perforated domains D^ϵ has been recently derived in [13, 14] and in the more general context of fluid flow in [15]. For porosity $p := \frac{|Y^1|}{|Y|}$, isotropic mobility $\hat{\mathrm{M}} = m\,\{\delta_{ij}\}_{1\le i,j\le d}$ with $m>0$, and δ_{ij} the Kronecker delta, equation (12) turns after upscaling ($\epsilon \to 0$) into the following problem defined on the homogeneous domain D, that is,

$$(\mathbf{M}^0) \qquad \begin{cases} p\frac{\partial \phi^0}{\partial t} = \mathrm{div}\left(m\hat{\mathrm{D}}\nabla f_L(\phi^0)\right) - \frac{\lambda^2}{p}\mathrm{div}\left(m\hat{\mathrm{D}}\nabla\left(\mathrm{div}\left(\hat{\mathrm{D}}\nabla\phi^0\right)\right)\right) & \text{in } D_T := D\times(0,T)\,, \\ \mathbf{n}\cdot\nabla\phi^0 = 0 & \text{in } (\partial D)_T\,, \\ \mathbf{n}\cdot\nabla\Delta\phi^\epsilon = 0 & \text{in } (\partial D)_T \end{cases} \tag{15}$$

where the effective tensor $\hat{\mathrm{D}} := \{d_{i,k}\}_{1\le i,k\le d}$ is defined by

$$d_{ij} := \sum_{k=1}^{d} \mathcal{M}_{Y^1}\left(\delta_{ij} - \delta_{ik}\frac{\partial \xi^j}{\partial y_k}\right) := \frac{1}{|Y|}\sum_{k=1}^{d}\int_{Y^1}\left(\delta_{ij} - \delta_{ik}\frac{\partial \xi^j}{\partial y_k}\right)\,d\mathbf{y}\,. \tag{16}$$

The correctors ξ^k, $1\le k\le d$ solve the following well-known elliptic reference cell problems which account for the geometry of the perforation identified by a characteristic (and periodic) pore space $Y^1\subset(0,1)^d$, i.e.,

$$\begin{cases} -\sum_{i,j=1}^{d}\frac{\partial}{\partial y_i}\left(\delta_{ij}\left(\frac{\partial(y_k-\xi^k)}{\partial y_j}\right)\right) = 0\,, & \text{in } (Y^1)_T\,, \\ \sum_{i,j=1}^{d}\mathrm{n}_i\left(\delta_{ij}\frac{\partial(y_k-\xi^k)}{\partial y_j}\right) = 0 & \text{on } (\partial Y^1)_T\,, \\ \xi^k(\mathbf{y}) \text{ is } Y^1\text{-periodic and } \mathcal{M}_{Y^1}(\xi^k) = 0\,, \end{cases} \tag{17}$$

where $y_k := \mathbf{y}\mathbf{e}_k$ and $\mathbf{e}_k$ is the canonical basis in $\mathbb{R}^d$.

The homogenized equation (15) is obtained in [14] with the help of the multiple scale expansion method wich is based on the ansatz of a two-scale expansion of the form

$$\phi^\epsilon = \phi^0(\mathbf{x},\mathbf{y},t) + \epsilon\phi^1(\mathbf{x},\mathbf{y},t) + \epsilon^2\phi^2(\mathbf{x},\mathbf{y},t) + \cdots\,. \tag{18}$$

This leads then to a sequence of problems where a solvability constraint on the third problem (i.e., the one defining ϕ^2) provides the upscaled equation.

Remark 2. *1. A consequence of the concept of LTE and the linearization of the nonlinear free energy density around the homogenized/upscaled order parameter ϕ^0 in the homogenization process, i.e., $f(\phi^\epsilon) = f(\phi^0) + f'(\phi^0)(\phi^\epsilon-\phi^0) + \ldots$, is that we end up the classical (linear) cell problem (17).*
2. We note that the homogenized formulation (15) holds true for the general case where the interfacial width is smaller than the material's characteristic/average pore size ℓ. This case is frequently observed in real applications where it generally holds true that solid-fluid and fluid-fluid interfaces are much smaller than the pore size. If this would not be the case, then such materials would not be attractive for applications since they require too much energy to pump fluids through such a medium. In fact, the scenario of interfacial widths being smaller than ℓ is a general working assumption in porous media modelling, and it also guarantees the well-accepted and widely used LTE property [40, 41, 42, 43].

Fluctuations: Langevin dynamics $(\mathbf{L}^\epsilon)$. Let $(\Omega,\mathcal{F},\mathrm{P})$ denote a probability space. We introduce a random force $\eta^\epsilon(\mathbf{x},t;\omega)\,:\,D^\epsilon\times(0,T)\times\Omega\to\mathbb{R}$ of the form

$$\begin{aligned} \langle\eta^\epsilon(\mathbf{x},t),\eta^\epsilon(\mathbf{x}',t')\rangle &= \delta(\mathbf{x}-\mathbf{x}')\delta(t-t')\,, \\ \langle\eta^\epsilon(\mathbf{x},t)\rangle &= 0\,, \end{aligned} \tag{19}$$

which accounts for loss of information by the coarse graining [36]. By the fluctuation-dissipation theorem [44], thermal fluctuations enter by adding the product of the parameter $\sigma(\theta) := \sqrt{2k_B\theta M} = \sqrt{2D}$ with η^ϵ to the microscopic formulation $\mathbf{(M^\epsilon)}$. The variable θ is the temperature and k_B the Boltzmann constant and hence the mobility $\mathrm{M} = \frac{\mathrm{D}}{k_B\theta}$ is linked to the diffusion constant D via Einstein's relation. η^ϵ is generally assumed to be Gaussian and uncorrelated (white). This leads to the conserved Langevin dynamics of the Ginzburg-Landau/Cahn-Hilliard equation (4)

$$\mathbf{(L^\epsilon)} \qquad \begin{cases} \partial_t \phi^\epsilon = \operatorname{div}\left(\mathrm{M}\nabla\left(f_L'(\phi^\epsilon) - \lambda\Delta\phi^\epsilon\right)\right) + \sigma(\theta)\eta^\epsilon\,, & \text{in } (D^\epsilon)_T\,, \\ \mathbf{n}\cdot\nabla\phi^\epsilon = 0\,, & \text{on } (\partial D^\epsilon)_T\,, \\ \mathbf{n}\cdot\nabla\Delta\phi^\epsilon = 0\,, & \text{on } (\partial D^\epsilon)_T\,. \end{cases} \tag{20}$$

3. Numerical schemes and convergence

The subsequent spatial discretizations of the three phase field formulations $\mathbf{(M^\epsilon)}$, $\mathbf{(M^0)}$, and $\mathbf{(L^\epsilon)}$ rely on the linear finite element method [45]. We perform all the computations on the unit square $D := [0,1]^2$.

3.1. Numerical schemes

We computationally investigate the influence of periodic porous media with three different numerical schemes: discretization $\mathbf{(M^{\epsilon,l}_{h,k})}$ represents a classical finite element discretization fully resolving perforated domains D^ϵ. Scheme $\mathbf{(M^{0,l}_{h,k})}$ is a linear finite element approximation of the upscaled/homogenized phase field formulation (15) recently derived in [13, 15]. Finally, with the discretization $\mathbf{(L^{\epsilon,l}_{h,k})}$ we consider the influence of thermal fluctuations and different perforations characterized by pore geometry $Y^1 \subset Y$, porosity p, and heterogeneity ϵ.

We denote a quasi-uniform triangulation of the bounded polygonal domain $D^\epsilon \subset \mathbb{R}^d$ into triangles or tetrahedrons by $\mathcal{T}_h$ for $d = 2$ and $d = 3$, respectively. The parameter $h > 0$ denotes the mesh size. The set of all nodes of $\mathcal{T}_h$ is $\mathcal{N}_h := \{\mathbf{z}_j\}_{j=1}^J$. We define the linear finite element space by

$$V_h := \left\{ \phi \in C(\overline{D}^\epsilon) \,\middle|\, \phi\big|_K \in P_1(K),\, K \in \mathcal{T}_h \right\}.$$

Let $\{\varphi_j\}_{j=1}^J$ be the nodal basis of V_h. This allows us to define the nodal interpolation operator $I_h : C(\overline{D}^\epsilon) \to V_h$ such that $I_h[u] = \sum_{j=1}^J u(\mathbf{z}_j)\varphi_j(\mathbf{x})$ for $u \in C(\overline{D}^\epsilon)$. For a given time-step size $k > 0$, the variable $n \in \mathbb{N}_0$ with $0 \le n \le N$, denotes discrete time-steps referring to the associated physical time $t_n = nk$ such that $t_N = T$ is the final time-step. Let $\phi^\epsilon_{h,k} := \sum_j^J \phi_j^n \varphi_j(\mathbf{x})$ denote the finite element approximation of ϕ^ϵ. Hence, we subsequently gather the coefficients ϕ_j^n in the vector $\boldsymbol{\phi}^\epsilon_n := \left\{\phi_j^n\right\}_{j=1}^J$. Finally, the we will frequently use the L^2-scalar product denoted by $(u,v) := \int_U uv\,d\mathbf{x}$ for domains $U \in \{D, D^\epsilon\}$.

Discretization of the microscopic problem $\mathbf{(M^\epsilon)}$. We discretize the microscopic problem $\mathbf{(M^\epsilon)}$ by mixed linear finite elements in space [45] and we compute numerical approximations in time by the θ-method which generalizes Crank-Nicholson's method ($\theta = 1/2$) [46] to arbitrary $0 < \theta < 1$. First, we identify for $1 \le i,j \le d$ the mass matrix by $\mathbb{M} := \{m_{ij}\}_{i,j=1}^J$, $m_{ij} := (\varphi_i, \varphi_j)$, the stiffness matrix by $\mathbb{S} := \{s_{ij}\}_{i,j=1}^J$, $s_{ij} := (\nabla\varphi_i, \nabla\varphi_j)$, and the nonlinear matrix by $\mathbb{K}(\boldsymbol{\phi}^{\epsilon,l}_{n+1}) := \left\{k_{ij}(\boldsymbol{\phi}^{\epsilon,l}_{n+1})\right\}_{i,j=1}^J$, $k_{ij}(\boldsymbol{\phi}^{\epsilon,l}_{n+1}) := \left(\left(\boldsymbol{\phi}^{\epsilon,l}_{n+1}\right)^2 \varphi_i, \varphi_j\right)$. Herewith, we can write the following mixed finite element

$$\mathbf{(Scheme\ M^{\epsilon,l}_{h,k})} \quad \begin{cases} \mathbb{M}\boldsymbol{\phi}^{\epsilon,l+1}_{n+1} + km\mathbb{S}\boldsymbol{\mu}^{\epsilon,l+1}_{n+\theta} = \mathbb{M}\boldsymbol{\phi}^\epsilon_n\,, \\ \mathbb{M}\boldsymbol{\mu}^{\epsilon,l+1}_{n+\theta} + \mathbb{K}(\boldsymbol{\phi}^{\epsilon,l}_{n+1})\boldsymbol{\phi}^{\epsilon,l+1}_{n+1} - \frac{1}{2}\mathbb{M}\boldsymbol{\phi}^{\epsilon,l+1}_{n+1} - \lambda\mathbb{S}\boldsymbol{\phi}^{\epsilon,l+1}_{n+1} = 0\,, \end{cases} \tag{21}$$

for the polynomial free energy density $f(\phi) = 1/4\phi^2(1-\phi)^2$ and the coefficient vectors $(\boldsymbol{\phi}_n^{\epsilon,l}, \boldsymbol{\mu}_n^{\epsilon,l})$, where $\boldsymbol{\phi}_n^{\epsilon,l} := \left\{\phi_{j,n}^{\epsilon,l}\right\}_{j=1}^{J}$ represents the order parameter of the immiscible mixture and $\boldsymbol{\mu}_n^{\epsilon,l} := \left\{\mu_{j,n}^{\epsilon,l}\right\}_{j=1}^{J}$ the discretized chemical potential μ (see Defintion 1), of the finite element functions $(\phi_{h,n}^{\epsilon,l}, \mu_{h,n}^{\epsilon,l}) \in V_h \times V_h$, that is, $u_{h,k}^{\epsilon,l} := \sum_{j=1}^{J} u_{j,n}^{\epsilon,l}\varphi_j(\mathbf{x})$ for $u \in \{\phi, \mu\}$. The index $l \in \mathbb{N}$, $0 \leq l \leq L$, denotes the iteration level in the scheme $\mathbf{M}_{h,k}^{\epsilon,l}$ linearized by a fixed point iteration. The iteration is based on Newton's method. Scheme $\mathbf{M}_{h,k}^{\epsilon,l}$ consists of the θ-method which is a result of defining $\boldsymbol{\mu}_{n+\theta}^{\epsilon,l+1} := (1-\theta)\boldsymbol{\mu}_n^{\epsilon} + \theta\boldsymbol{\mu}_{n+1}^{\epsilon,l+1}$ for $0 \leq \theta \leq 1$. As noted earlier, we set $\theta = 0.5$.

Discretization of the effective macroscopic problem $(\mathbf{M}^0)$. The computation of the phase field formulation $(\mathbf{M}^0)$ requires to modify scheme $\mathbf{M}_{h,k}^{\epsilon,l}$ to include the porous media correction tensor $\hat{\mathrm{D}}$ which needs for a specific pore geometry Y^1 the additional computation of the reference cell problem (17). If we denote the stiffness matrix defined on the domain Y^1 again by $\mathbb{S}$, which is accordingly defined as in (21) above, then the cell problem (17) for ξ^k turns into the discrete numerical

$$\textbf{(Scheme Y)} \quad \left\{ \quad \mathbb{S}\tilde{\boldsymbol{\xi}}^k = \mathbf{0}\,, \right. \tag{22}$$

where $\tilde{\boldsymbol{\xi}}^k := \left\{\tilde{\xi}_j^k\right\}_{j=1}^{J}$, $0 \leq k \leq d$, is the vector of the coefficients $\tilde{\xi}_j^k := \xi^k - y_k$, of the finite element solution $\tilde{\xi}_h^k := \sum_{j=1}^{d} \tilde{\xi}_j^k \varphi_j(\mathbf{y})$, $\mathbf{y} \in Y^1$. We note that $\tilde{\boldsymbol{\xi}}^k$ is only unique up to a constant which is uniquely defined by the zero-average constraint $(17)_3$. Despite the fact that scheme $\mathbf{Y}$ is a classical elliptic problem, the efficient and reliable solution of (22) for complex/highly complicated pore geometries leads often to a formidable, high-dimensional problem due to the necessity of fine grids.

Herewith, we can compute the porous media corrector coefficients d_{ij} by standard quadrature over the pore space $Y^1 \subset Y$. This allows us then to introduce discrete versions of upscaled operators such as the effective stiffness matrix $\overline{\mathbb{S}} := \{\overline{s}_{ij}\}_{i,j=1}^{J}$, $\overline{s}_{ij} := \left(\hat{\mathrm{D}}\nabla\varphi_i, \nabla\varphi_j\right)$. The linear finite element approximations $(\phi_{n,h}^0, \mu_{n,h}^0) \in V_h \times V_h$ for solutions of the effective/upscaled phase field formulation $(\mathbf{M}^0)$ (eq. (15)) are then obtained as the solutions of the following

$$\textbf{(Scheme } \mathbf{M}_{h,k}^{0,l}\textbf{)} \quad \left\{ \begin{array}{l} p\mathbb{M}\boldsymbol{\phi}_{n+1}^{0,l+1} + km\overline{\mathbb{S}}\boldsymbol{\mu}_{n+\theta}^{0,l+1} = p\mathbb{M}\boldsymbol{\phi}_n^0\,, \\ \mathbb{M}\boldsymbol{\mu}_{n+\theta}^{0,l+1} + \mathbb{K}(\phi_{n+1}^{0,l})\boldsymbol{\phi}_{n+1}^{0,l+1} - \frac{1}{2}\mathbb{M}\boldsymbol{\phi}_{n+1}^{0,l+1} - \frac{\lambda}{p}\overline{\mathbb{S}}\boldsymbol{\phi}_{n+1}^{0,l+1} = 0\,. \end{array} \right. \tag{23}$$

Discretization of the Langevin equation $(\mathbf{L}^{\epsilon})$. The additive white noise term η^{ϵ} in $(\mathbf{L}^{\epsilon})$ requires us to extend the numerical scheme $\mathbf{A}^{\epsilon}$. Since η^{ϵ} is uncorrelated, we can approximate it as a cylindrical Wiener process (space-time white noise) [47], i.e.,

$$\eta(\mathbf{x}, t) = \sum_{j=1}^{\infty} \beta_j(t_n)\varphi_j(\mathbf{x})\,, \tag{24}$$

where the coefficients $\beta_j(t)$ are i.i.d. Brownian motions, i.e., $\beta_j(t_n) = \beta_j(t_{n-1}) + Z$, $Z \sim \mathcal{N}(0, k)$. This allows us to gather the coefficients β_j in the vector $\boldsymbol{\beta}_n := \{\beta_{j,n}\}_{j=1}^{J}$. Based on these definitions we can numerically approximate solutions of (20) by iterates $(\boldsymbol{\phi}_{n+1}^{\epsilon,l+1}, \boldsymbol{\mu}_{n+1}^{\epsilon,l+1})$ solving the following

$$\textbf{(Scheme } \mathbf{L}_{h,k}^{\epsilon,l}\textbf{)} \quad \left\{ \begin{array}{l} \mathbb{M}\boldsymbol{\phi}_{n+1}^{\epsilon,l+1} + km\mathbb{S}\boldsymbol{\mu}_{n+\theta}^{\epsilon,l+1} = \mathbb{M}\boldsymbol{\phi}_n^{\epsilon} + \sigma(\theta)\mathbb{M}\boldsymbol{\beta}_n\,, \\ \mathbb{M}\boldsymbol{\mu}_{n+\theta}^{\epsilon,l+1} + \mathbb{K}(\boldsymbol{\phi}_{n+1}^{\epsilon,l})\boldsymbol{\phi}_{n+1}^{\epsilon,l+1} - \frac{1}{2}\mathbb{M}\boldsymbol{\phi}_{n+1}^{\epsilon,l+1} - \lambda\mathbb{S}\boldsymbol{\phi}_{n+1}^{\epsilon,l+1} = 0\,, \end{array} \right. \tag{25}$$

where $\sigma(\theta)$ accounts for thermal fluctuations and hence it is a constant coefficient which dependes on the temperature θ.

3.2. Convergence of solutions of **Scheme** $\mathbf{M}_{h,k}^{\epsilon,l}$ *to solutions of* **Scheme** $\mathbf{M}_{h,k}^{0,l}$ *for* $\epsilon \to 0$

We computationally study the error behaviour between the solution of the microscopic (12) and the solution of the macroscopic equation (15). In a recent article [30], the following rigorous error quantification is derived:

Theorem 1. (Error estimates) *Assume smooth enough data (see [30, Assumption C]) and a Lipschitz boundary* $\partial\Omega^\epsilon$ *with interface* $I_\Omega^\epsilon := \partial\Omega^\epsilon \cap \partial B^\epsilon$.[2] *Let* $\hat{\mathrm{M}} = m\hat{\mathrm{I}}$ *be an isotropic mobility with* $\hat{\mathrm{I}}$ *representing the identity matrix. Let* ϕ^ϵ *be a solution of (12), or equivalently* ϕ^ϵ *and* w^ϵ *solve the splitting formulation*

$$\begin{cases} \partial_t(-\Delta)^{-1}w^\epsilon - \lambda \mathrm{div}\left(\hat{\mathrm{M}}\nabla w^\epsilon\right) = \mathrm{div}\left(\frac{\hat{\mathrm{M}}}{\lambda}\nabla f_L(\phi^\epsilon)\right) & \text{in } (\Omega^\epsilon)_T\,, \\ \nabla_n w^\epsilon = -\nabla_n \Delta\phi^\epsilon = 0 & \text{on } (\partial\Omega^\epsilon)_T\,, \\ -\Delta\phi^\epsilon = w^\epsilon & \text{in } (\Omega^\epsilon)_T\,, \\ \nabla_n \phi^\epsilon = 0 & \text{on } (\partial\Omega^\epsilon)_T\,, \\ \phi^\epsilon(\mathbf{x},0) = \psi(\mathbf{x}) & \text{in } \Omega^\epsilon\,. \end{cases} \tag{26}$$

If the free energy F *is polynomial, then the error variables* $\mathrm{E}_\epsilon^\phi := \phi^\epsilon - (\phi_0 + \epsilon\phi_1)\,, \mathrm{E}_\epsilon^w := w^\epsilon - (w_0 + \epsilon w_1)$, *where* $w_1 := -\sum_{k=1}^d \xi_w^k(\mathbf{y})\frac{\partial w_0}{\partial x_k}(\mathbf{x},t)$ *and* $\phi_1 := -\sum_{k=1}^d \xi_\phi^k(\mathbf{y})\frac{\partial \phi_0}{\partial x_k}(\mathbf{x},t)$, *satisfy for* $0 \le t \le T$ *and* $0 < T < \infty$ *the following estimates*

$$\begin{aligned} \|E_\epsilon^w(\cdot,t)\|_{L^2(\Omega^\epsilon)}^2 + c(m,\lambda,\kappa)\int_0^t \|\mathcal{A}_\epsilon E_\epsilon^w(\cdot,s)\|_{L^2(\Omega^\epsilon)}^2\,ds \\ \le \epsilon^{1/2} C(T,\Omega,m,\kappa,\lambda)\,, \\ \left\|E_\epsilon^\phi(\cdot,t)\right\|_{H^1(\Omega^\epsilon)} \le \epsilon^{1/4} C(T,\Omega,m,\kappa,\lambda)\,, \end{aligned} \tag{27}$$

where $c(m,\lambda,\kappa)$ *and* $C(T,\Omega,m,\kappa,\lambda)$ *are constants independent of* $\epsilon := \frac{\lambda}{L}$.

Remark 3. *We note that the proof of the above Theorem 1 does not take the error behaviour in the boundary region into account by using a smooth truncation. This leads for linear elliptic equations to the by now classical convergence rate* $\mathcal{O}(\epsilon^{1/2})$, *e.g. [48, 49]. However, in recent attempts [50, 51], the authors can improve the convergence rates with the help of operator estimates with a resulting rate* $\mathcal{O}(\epsilon)$ *for 2nd order elliptic equations. We note, that our estimates in (27) are derived based on the classical method but due to the fourth order operator, we end up with the slightly lower rate* $\mathcal{O}(\epsilon^{1/4})$, *albeit under the generally required strong regularity [30, Assumption C]. The strongest regularity result currently available seems to be the bounds derived in [52].*

Since the error estimates grow in time and since the (exact) initial conditions are defined on the perforated domain, there will be a very short relaxation time with the numerical Scheme $(\mathbf{M}_{h,k}^0)$ of the homogenized problem and hence we computationally investigate the error after the first 5 time steps for vanishing heterogeneity ($\epsilon \to 0$) and for two different pore geometries, i.e., a circle (centered with radius $\epsilon/5$) and a square (centered with edge length $\epsilon/5$). In particular, we numerically compute the following error $e_{5,h} := \|\phi_{5,h}^\epsilon - \phi_{5,h}^0\|_{L^2(D^\epsilon)}$ with respect to the perforated domain D^ϵ, where $\phi_{5,h}^\epsilon$ and $\phi_{5,h}^0$ are the linear finite element solutions of the **Scheme** $\mathbf{M}_{h,k}^{\epsilon,l_f}$ approximating the microscopic problem $(\mathbf{M}^\epsilon)$ and of the **Scheme** $\mathbf{M}_{h,k}^{0,l_f}$ approximating the homogenized problem $(\mathbf{M}^0)$, respectively, where l_f indicates in both cases the smallest number of iterations to satisfy a pre-defined tolerance in the nonlinear solver (note that l_f is not necessarily equal for these two schemes). Fig. 2 (left) shows a convergence rate of $\mathcal{O}(\epsilon)$ for square-shaped

[2] see [48] for instance

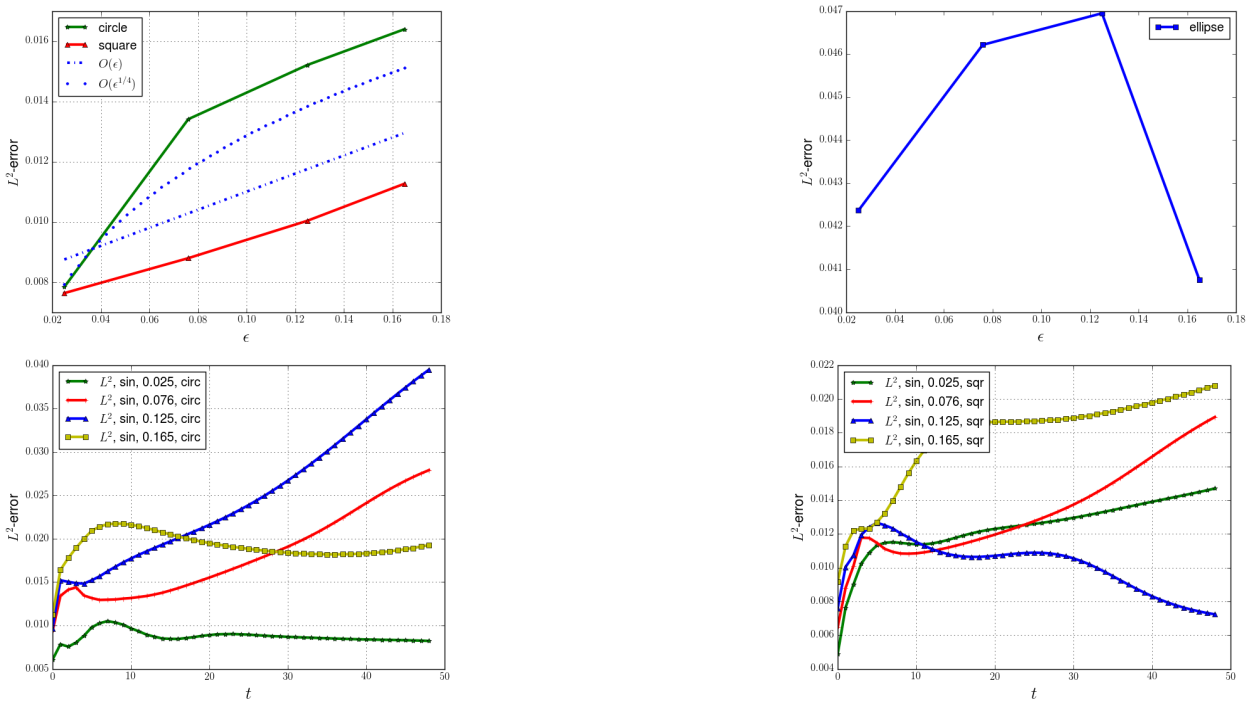

Figure 2: **Top line:** Convergence (**left**) (for $\epsilon = 0.025, 0.076, 0.125, 0.165$) for circular and square-shaped perforations. Picture on the (**right**) shows the L^2-error for elliptical perforations. Errors for $\epsilon = 0.125, 0.165$ are in the pre-asymptotic regime since different mesh sizes lead to the same qualitative result. **Bottom line:** Evolution of the error for circular (**left**) and square-shaped (**right**) perforations.

perforations and of $\mathcal{O}(\epsilon^{1/4})$ for circular perforations under the fixed mesh size $h \approx 1/100$.[3] The geometric dependence of the convergence rates depicted in Fig. 2 mainly arises for the following two reasons:

(R1) geometry and regularity of the boundary influence the size of the estimated error bound (i.e., the constant involved in the estimate applying a truncation argument [55]);

(R2) discretization(/triangulation (2D)) of the boundary geometry: the resolution of curved boundaries generally requires a larger number of grid points to properly resolve the curvature than flat boundaries.

In particular, classical error estimates for elliptic problems in homogenization rely on a truncation argument near the boundary as well as the computational approximation thereof, i.e., reason (R2) about curved boundary geometries, together suggest that the additional error induced by the truncation in such error estimates is compensated by the higher resolution (higher number of grid points) of curved boundaries and hence the computed convergence rate for circular geometries agrees with the theoretical upper bound in Fig. 2. Therefore, we recommend for the computational error investigation to use perforations that show flat and not curved surfaces. We also note that refined error estimates not using the classical truncation argument but relying on spectral estimates have recently been developed in [50, 51] for instance. These novel error bounds show a linear convergence rate for elliptic problems such as the Poisson equation.

We also provide plots of the error behaviour over time in Fig. 2, middle and right, which does not allow us to deduce an evolutionary behaviour of the error. We note that theoretically one has currently an evolutionary error bound (27) based on Gronwall's inequality. Here it would be interesting to investigate whether a time independent error bound can be derived.

[3] These computational results depend on meshes created for different heterogeneities ϵ but fixed number of degrees of freedom. A convenient tool is the mesh generator of the open source package mshr [53] which is part of the finite element library FEniCS [54].

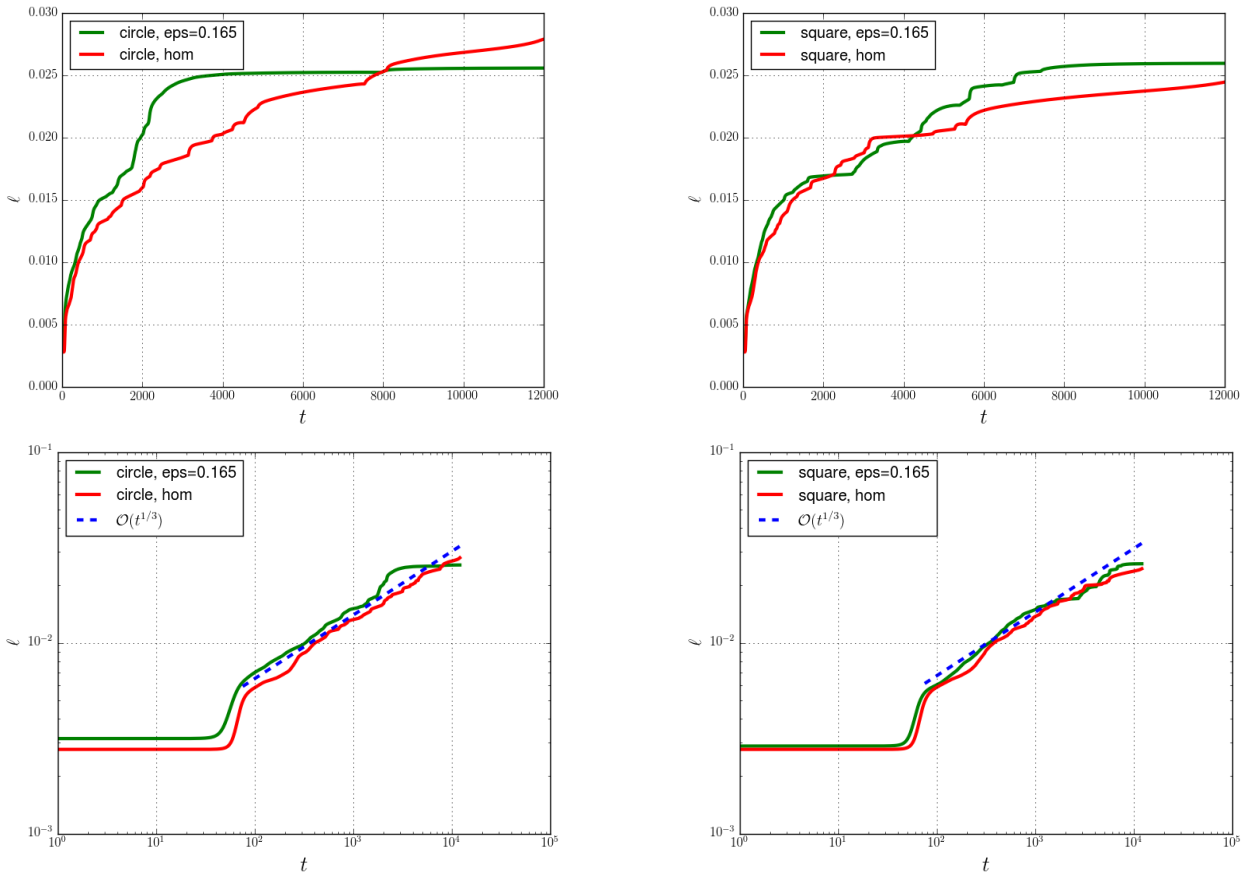

Figure 3: Influence of porosity on the coarsening rate. The universal growth rate $\mathcal{O}(\epsilon^{1/3})$ is recovered in the porous media setting [36, 32, 33].

4. Interfacial dynamics under perforations: coarsening rates

4.1. Influence of the pore geometry and porosity

The subsequent computations are devoted to the investigation of the influence of pore geometries on the coarsening rate [33] under fixed porosity ($p = 0.5$) and heterogeneity ($\epsilon = 0.165$). The numerical results are obtained with the schemes $\mathbf{M}^{\epsilon,l}_{h,k}$ and $\mathbf{M}^{0,l}_{h,k}$ providing time (k) and space (h) discrete solutions of the microscopic phase field problem $\mathbf{M}^{\epsilon}$ and the corresponding homogenized/upscaled formulation $\mathbf{M}^{0}$, respectively. We depicted the results in Fig. 3 for a circular (left) and a square (right) pore geometry. The two numerical schemes $\mathbf{M}^{\epsilon,l}_{h,k}$ and $\mathbf{M}^{0,l}_{h,k}$ show qualitatively the same coarsening rate for both geometries. The slightly better approximation of the homogenized solution for square shaped pores is in part due to the more complex mesh generation of domains with curved boundaries and due to the difficulty to control the number of degrees of freedom with the mesh generator mshr as part of the open source project FEniCS, see [53] and [54].

Next, we are interested in the influence of thermal fluctuations on the coarsening rate. Let us note that in the study of dynamic interfaces in disordered media [56], one is mainly interested in so-called *quenched noise* which differs from *thermal noise* by its origin in the disorder of the medium and hence the temporal dependance in *thermal noise* is replaced by a dependance of the *quenched noise* on the system's state/order parameter ϕ. However, we do not study random porous media in this article and hence the stochastic Cahn-Hilliard equation (20) is driven by *thermal noise*. To this end, we employ the Langevin formulation $\mathbf{L}^{\epsilon}$

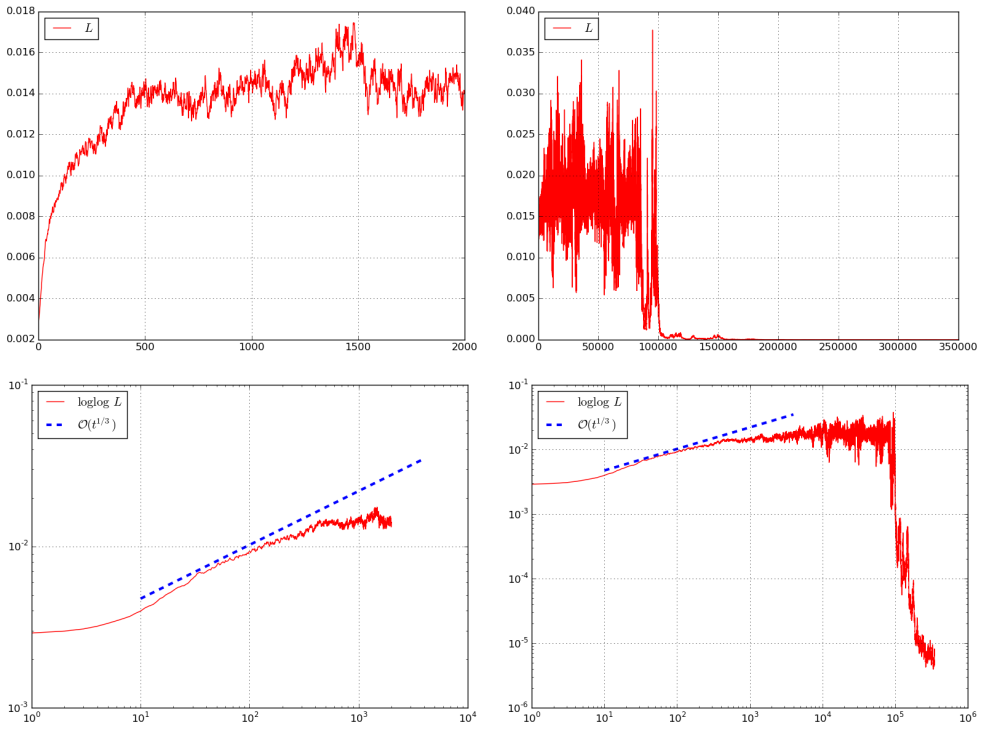

Figure 4: Coarsening in a circular porous medium for the Langevin formulation (25) for critical quenches. Characteristic length $L = 1/f(\phi)$ for the first 2000 time steps **(top left)** and according loglog plot **(bottom left)**. Characteristic length for 3500 time steps **(top right)** and according loglog plot **(bottom right)**.

which is discretized by the scheme $\mathbf{L}_{h,k}^{\epsilon,l}$. We additionally impose random initial conditions of the form

$$\phi(\mathbf{x}, 0) = 0.5 + w(0.5 + r_{\mathbf{x}}) \,, \tag{28}$$

where $r_{\mathbf{x}} \in [0, 1]$ stands for random fluctuations with mean value zero and is imposed on each spatial point $\mathbf{x} \in \mathcal{D} = (0, 1)^2$. The parameter $w > 0$ weights the influence of noise. Its default value is $w = 0.125$. Note that the mean value 0.5 of the initial condition (28) introduces *critical quenches* since the equilibrium limiting values of the free energy density (6) are 0 and 1. We note that the term "quenching" has its origin in the thermodynamic description of phase separation. In particular, the Cahn-Hilliard formulation describes well the case of "quick quenching" where a given initial temperature θ_0 is rapidly lowered to $\theta_1 \ll \theta_0$. Let $\overline{\phi}$ denote a uniform/homogeneous composition throughout the domain D enclosed by no-flux boundary conditions. Based on this, a phase diagram, which depicts the locations of the order parameter ϕ and the temperature θ on separate axes, allows us to determine whether the system has undergone a phase separation or not. That means, the system shows phase separation if the initial state $(\overline{\phi}, \theta_0)$ lies above the coexistence curve (binodal) and the quenched state $(\overline{\phi}, \theta_1)$ below the binodal curve, see [57]. We recall that the binodal represents the condition where two distinct phases may coexist. For instance, in binary mixtures the coexistence curve represents the tangent line to the associated free energy.

The term "critical quenches" describes the case where the system evolves through the critical point $(\overline{\phi}_c, \theta_c)$ during the process of "quick quenching" described above, i.e., "quick quenching" happens for $\overline{\phi} = \overline{\phi}_c$. In this case, the universal scaling $\mathcal{O}(t^{1/3})$ of the coarsening phenomenon does not necessarily hold due to the formation of percolating phases, which can also be seen in the rather complex dynamics depicted in Fig. 4. A noteworthy feature of coarsening under fluctuations is the sudden decrease of the size L of the characteristic domain size L in Fig. 4 (right) after large enough times.

Finally, we compute the evolution of interfaces in a domain $D = [0, 1]^2$ with circular perforations under the

homogenized scheme (23) for various porosities $p = \frac{|Y^1|}{|Y|}$ and external forcings F imposed as flux boundary conditions, i.e., $\nabla\mu\cdot\mathbf{n} = -F$ on the left entry and $\nabla\mu\cdot\mathbf{n} = F$ on the right exit where $\mathbf{n}$ is the outward normal and μ the chemical potential. A half circle with barycenter located in the middle of the left boundary forms the initial condition. Four different time steps showing locations of the interfaces for specific forces F can be found in Fig. 5. We also investigate the interfacial motion under different applied forces for the microscopic formulation (21) where the pore space is fully resolved. Interestingly, for externally applied forces of $F = 0.01$ up to $F = 10000$, we did not experience any differences in the interfacial evolution for constant porosity $p = 0.5$. Hence, we analyse the influence of different porosities under a fixed external forcing of $F = 10000$. The results are depicted in Fig. 6. As one can see in Fig. 6, the lower the porosity of the perforated medium is, the more discrete is behaviour of the interface. We also note that the interface advances faster under lower porosities (compare the interface locations for $p = 0.3$ (white) and $p = 0.9$ (diffuse interface) in Fig. 6 for instance). In fact, the interfacial width is larger or equal to the smallest distance between the circular pore walls (which is the favorable interfacial location) for a porosity of $p = 0.3$, Fig. 6 (top row), and hence the interface, which tends to decrease its area, is unstable in its energetically favorable position. Hence, small perturbations in the composition ϕ cause the interface to move. In fact, the interface computed under $p = 0.9$ does not visibly move during the investigated 600 time steps. Moreover, the interfacial movements do not show monotonic behaviour with respect to the porosity. This effect is in part due to a pinning and de-pinning mechanism of the interface on the pore walls. In the phase field formulation (12), this mechanism can be controlled by the wetting boundary condition $(12)_2$.

5. Conclusion

We computationally investigate the recently derived upscaled/homogenized phase field equation (15) together with the associated microscopic formulation (12) which fully resolves domain specific heterogeneities. Our computations validate the rigorously derived convergence rate $\mathcal{O}(\epsilon^{1/4})$ for circles and show the even better rate $\mathcal{O}(\epsilon^1)$ for square pore geometries, see Fig. 2 (left). This results indicate that slightly higher convergence rates such as $\mathcal{O}(\epsilon)$ could be feasible by applying novel and more technical estimates such as the recently developed spectral estimates for second order elliptic equations [51, 50] in difference to the classical error estimates relying on a smooth truncation [48, 49, 58, 30] near the boundary. It is clear that computational results depend on the geometry of the perforation. Our observation between circular and square-shaped perforations suggests to use geometries with flat and not curved boundaries to study the error behaviour. The reason is that curved boundaries require a finer resolution/mesh than flat surfaces/boundaries. This makes the error analysis of computational results for homogenization problems more complex.

The time evolution of the upscaling/homogenization error (Fig. 2 middle and right) shows a complex dependence on the heterogeneity ϵ and the pore geometry. It is interesting to see that the effect of the porous medium leads in specific cases to a decrease in the error between the solution of the homogenized equation and the solution of the microscopic equation. Moreover, the time evolution of the homogenization error does not give a clear indication on the form of a possible sharp error bound in time. It would be of great interest to obtain sharp estimates in time in the future so that we can determine the exact temporal growth rate in (27), which relies on Gronwall's inequality.

Our investigation of the influence of pore geometry and heterogeneity on the coarsening of first-order phase separating systems recovers the experimentally and theoretically predicted universal behaviour, i.e., the $\mathcal{O}(t^{1/3})$-growth of characteristic domains with time t, see Fig. 3. By adding additive white noise to the microscopic formulation (12), see (20), we can also account for thermal fluctuations on the coarsening rate [36]. It is interesting to observe that the size of the characteristic domain behaves initially deterministic and then admits the fluctuations of the imposed white noise. Of particular interest is the sudden decrease of the size of the characteristic domain which appears after long enough evolution of the system, see Fig. 4 (right). To conclude, we note that for strongly heterogeneous media, i.e., heterogeneities below $\epsilon = 0.025$ (smallest value used in our comptutations), the upscaled/homogenized formulation is computationally favourable in view of computational time and storage (high dimensionality). Therefore, we believe that the effective

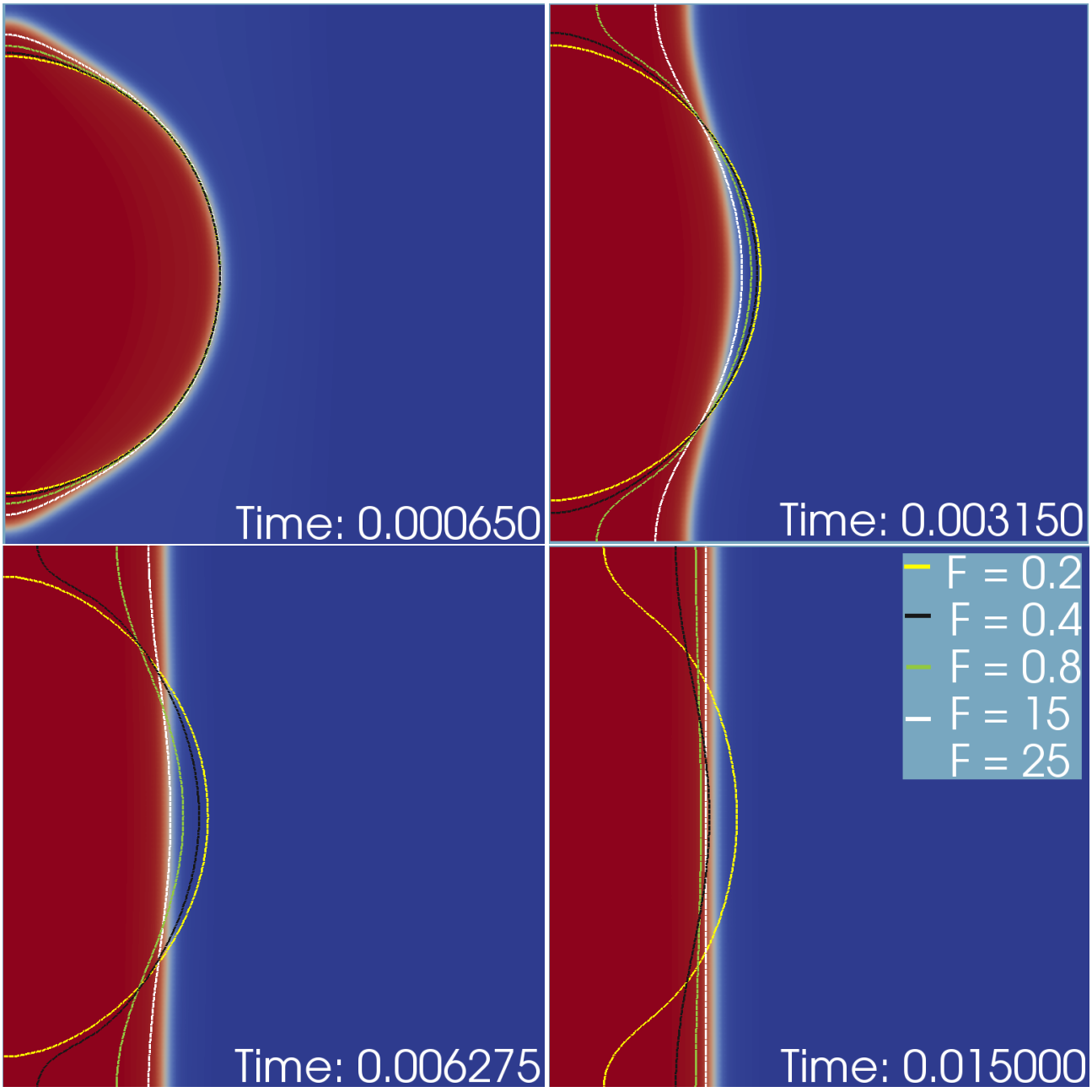

Figure 5: **Homogenized formulation:** Influence of forcings F on an advancing interface under constant porosity $p = 0.5$.

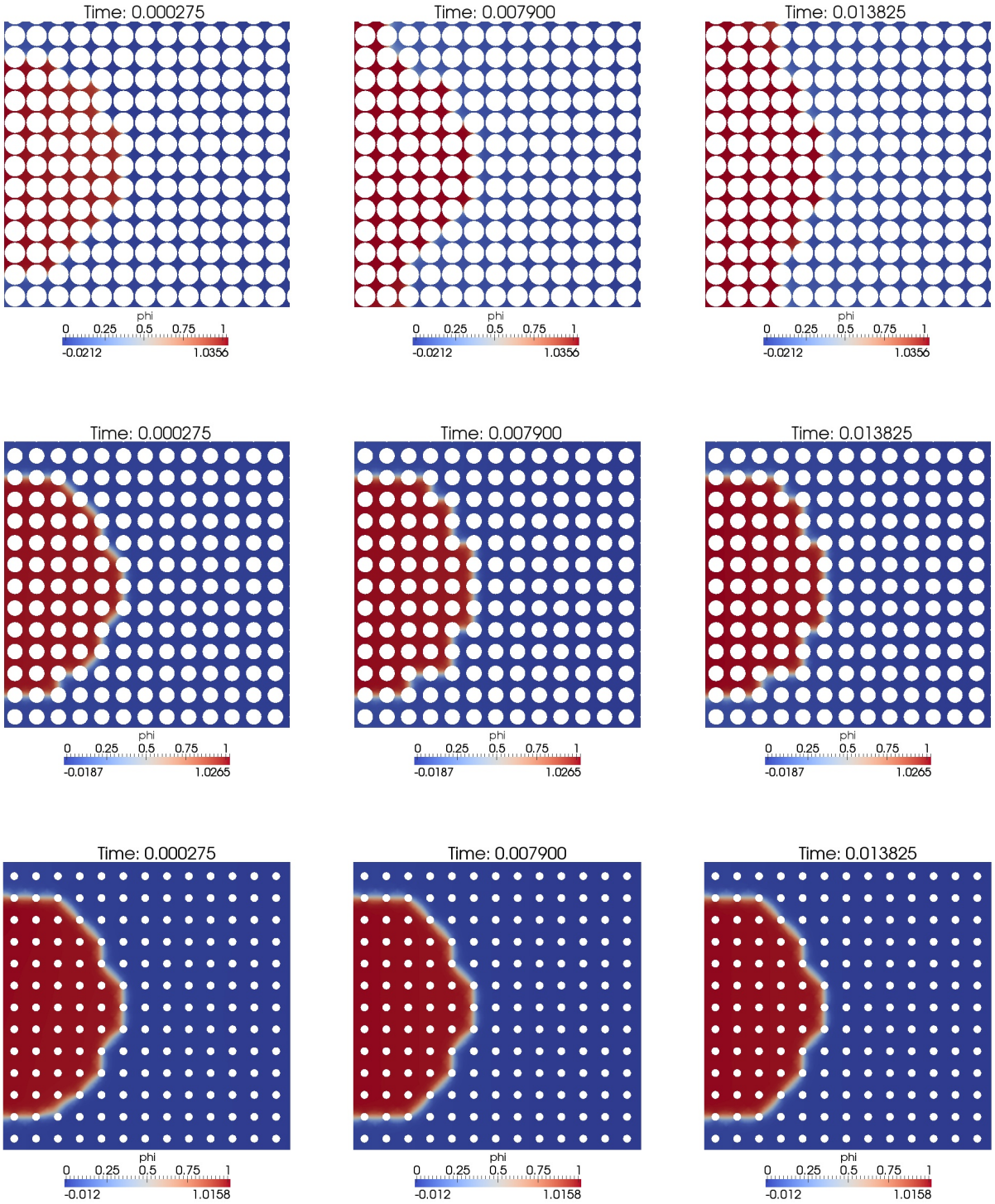

Figure 6: **Microscopic formulation:** Influence of porosity p on the advancing interface under constant influx and constant heterogeneity $\epsilon = 0.076$. Advancing interface displayed for different porosities and times: $p = 0.3$ (top row), $p = 0.6$ (middle row), and $p = 0.9$ (last row).

macroscopic Cahn-Hilliard formulation will be a promising tool for computational studies of various complex heterogeneous multiphase systems in science and engineering.

Acknowledgement
The first author was supported by The Maxwell Institute Graduate School in Analysis and its Applications, a Centre for Doctoral Training funded by the UK Engineering and Physical Sciences Research Council (grant EP/L016508/01), the Scottish Funding Council, Heriot-Watt University, and the University of Edinburgh. The second author received support from EPSRC under the grant EP/P011713/1.

Finally, we would like to thank the Reviewers for their helpful comments allowing us to refine the presentation of our results.

References

[1] J. Cahn, J. Hilliard, Free Energy of a Nonuniform System. I. Interfacial Free Energy, J. Chem. Phys. 28 (2) (1958) 258.
URL http://link.aip.org/link/JCPSA6/v28/i2/p258/s1&Agg=doi

[2] J. D. Van Der Waals, The thermodynamic theory of capillarity under the hypothesis of a continuous variation of density, Verhandel Konink. Akad. Weten. Amsterdam (Sec. 1) 1 (1892) 1–56. Translation by J. S. Rowlingson, 1979, *J. Stat. Phys.* 20,197–233.

[3] L. Evans, H. Soner, P. Souganidis, Phase transitions and generalized motion by mean curvature, Comm. Pure and Appl. Math. XLV (1992) 1097–1123.

[4] V. Slezov, Kinetics of First-order Phase Transitions, Wiley-VCH, 2009.

[5] D. Anderson, G. McFadden, A. Wheeler, Diffuse-interface methods in fluid mechanics, Ann. Rev.Fluid Mech. 30 (1998) 139–165.

[6] A. Lamorgese, D. Molin, R. Mauri, Phase field approach to multiphase flow modeling, Milan J. Math. 79 (2011) 597–642.

[7] P. Papatzacos, A Model for Multiphase and Multicomponent Flow in Porous Media, Built on the Diffuse-Interface Assumption, Transport in Porous Media 82 (3) (2009) 443–462. doi:10.1007/s11242-009-9405-2.
URL http://www.springerlink.com/index/10.1007/s11242-009-9405-2

[8] Valluri, P., Spelt, P.D.M., Lawrence, C.J., Hewitt, G.F., Numerical simulation of the onset of slug initiation in laminar horizontal channel flow, International Journal of Multiphase Flow 34 (2) (2008) 206–225. doi:10.1016/j.ijmultiphaseflow.2007.09.001.

[9] K. Promislow, B. Wetton, PEM fuel cells: a mathematical overview, SIAM J. Appl. Math. 70 (2) (2009) 369–409. doi:10.1137/080720802.
URL http://dx.doi.org/10.1137/080720802

[10] K. Promislow, N. Gavish, Nano-structured materials for fuel cells, SIAM News 45 (1).

[11] B. C. Han, a. Van der Ven, D. Morgan, G. Ceder, Electrochemical modeling of intercalation processes with phase field models, Electrochimica Acta 49 (26) (2004) 4691–4699. doi:10.1016/j.electacta.2004.05.024.
URL http://linkinghub.elsevier.com/retrieve/pii/S0013468604005213

[12] M. Z. Bazant, Z. P. Bazant, Theory of sorption hysteresis in nanoporous solids: Part II Molecular condensation, J. Mech. Phys. Solids 60 (2012) 1660–1675.

[13] M. Schmuck, M. Pradas, G. A. Pavliotis, S. Kalliadasis, Upscaled phase-field models for interfacial dynamics in strongly heterogeneous domains, Proc. R. Soc. A 468 (2147) (2012) 3705–3724. doi:10.1098/rspa.2012.0020.
URL http://rspa.royalsocietypublishing.org/cgi/doi/10.1098/rspa.2012.0020

[14] M. Schmuck, G. Pavliotis, S. Kalliadasis, Effective macroscopic interfacial transport equations in strongly heterogeneous environments for general homogeneous free energies, Appl. Math. Lett. 35 (2014) 12–17.

[15] M. Schmuck, M. Pradas, G. Pavliotis, S. Kalliadasis, Derivation of effective macroscopic Stokes–Cahn–Hilliard equations for periodic immiscible flows in porous media, Nonlinearity 26 (12) (2013) 3259.
URL http://stacks.iop.org/0951-7715/26/i=12/a=3259

[16] Nold, A., Sibley, D. N., Goddard, B. D., Kalliadasis, S., Nanoscale fluid structure of liquid-solid-vapour contact lines for a wide range of contact angles, Math. Model. Nat. Phenom. 10 (4) (2015) 111–125. doi:10.1051/mmnp/201510407.
URL http://dx.doi.org/10.1051/mmnp/201510407

[17] M. Pradas, N. Savva, J. B. Benziger, I. G. Kevrekidis, S. Kalliadasis, Dynamics of fattening and thinning 2d sessile droplets, Langmuir 32 (19) (2016) 4736–4745, pMID: 27077328. arXiv:http://dx.doi.org/10.1021/acs.langmuir.6b00256, doi:10.1021/acs.langmuir.6b00256.
URL http://dx.doi.org/10.1021/acs.langmuir.6b00256

[18] N. Savva, S. Kalliadasis, G. A. Pavliotis, Two-dimensional droplet spreading over random topographical substrates, Phys. Rev. Lett. 104 (2010) 84501.

[19] D. Sibley, A. Nold, S. Kalliadasis, The asymptotics of the moving contact line: cracking an old nut, Journal of Fluid Mechanics 764 (2015) 445–462. doi:10.1017/jfm.2014.702.
URL http://journals.cambridge.org/article_S0022112014007022

[20] J. Lowengrub, A. Rätz, A. Voigt, Phase-field modeling of the dynamics of multicomponent vesicles: Spinodal decomposition, coarsening, budding, and fission, Phys. Rev. E 79 (3) (2009) 31926.
URL http://link.aps.org/doi/10.1103/PhysRevE.79.031926

[21] S. Aland, A. Voigt, Benchmark computations of diffuse itnerface models for two-dimensional bubble dynamics, Int. J. Numer. Meth. Fluidsdoi:10.1002/fld.2611.

[22] C. Elliott, B. Stinner, V. Styles, R. Welford, Numerical computation of advection and diffusion on evolving diffuse interfaces, IMA Journal of Numerical Analysis 31 (3) (2010) 786–812. doi:10.1093/imanum/drq005.
URL http://imanum.oxfordjournals.org/cgi/doi/10.1093/imanum/drq005

[23] P. Gera, D. Salac, The cahn-hilliard-cook equation on curved surfaces in three-dimensional space, arXiv:1605.07108v1.

[24] D. B. Duncan, M. Grinfeld, I. Stoleriu, Coarsening in an integro-differential model of phase transitions, Euro. Journal of Applied Mathematics 11(6) (2000) 561–572.

[25] V. Heinonen, C. Achim, K. R. Elder, S. Buyukdagli, T. Ala-Nissila, Phase-field-crystal models and mechanical equilibrium, Phys. Rev. E 89 (2014) 032411.

[26] K. R. Elder, M. Katakowski, M. Haataja, M. Grant, Modeling elasticity in crystal growth, Phys. Rev. Lett. 88 (2002) 245701. doi:10.1103/PhysRevLett.88.245701.
URL http://link.aps.org/doi/10.1103/PhysRevLett.88.245701

[27] K. R. Elder, M. Grant, Modeling elastic and plastic deformations in nonequilibrium processing using phase field crystals, Phys. Rev. E 70 (2004) 051605. doi:10.1103/PhysRevE.70.051605.
URL http://link.aps.org/doi/10.1103/PhysRevE.70.051605

[28] E. Sandier, S. Serfaty, Limiting vorticities for the ginzburg-landau equations, Duke Math. J. 117 (3) (2003) 403–446.

[29] M. Dos Santos, P. Mironescu, O. Misiats, The ginzburglandau functional with a discontinuous and rapidly oscillating pinning term. part i: The zero degree case, Commun. Contemp. Math. 13 (5) (2011) 885–914.

[30] M. Schmuck, S. Kalliadasis, Rate of convergence of general phase field equations in strongly heterogeneous media towards their homogenized limit, preprint, https://arxiv.org/abs/1702.08292, submitted (2016).

[31] P. Yue, C. Zhou, J. Feng, Sharp-interface limit of the cahn-hilliard model for moving contact lines, J. Fluid Mech. 645 (2010) 279–294.

[32] K. R. Elder, R. C. Desai, Role of nonlinearities in off-critical quenches as described by the cahn-hilliard model of phase separation, Phys. Rev. B 40 (1989) 243–254. doi:10.1103/PhysRevB.40.243.
URL http://link.aps.org/doi/10.1103/PhysRevB.40.243

[33] V. R. Kohn, F. Otto, Upper bounds on coarsening rates, Communications in Mathematical Physics 229 (3) (2002) 375–395. doi:10.1007/s00220-002-0693-4.
URL http://dx.doi.org/10.1007/s00220-002-0693-4

[34] J. Zhu, L.-Q. Chen, J. Shen, V. Tikare, Coarsening kinetics from a variable-mobility cahn-hilliard equation: Application of a semi-implicit fourier spectral method, Phys. Rev. E 60 (1999) 3564–3572. doi:10.1103/PhysRevE.60.3564.
URL http://link.aps.org/doi/10.1103/PhysRevE.60.3564

[35] P. Fratzl, J. L. Lebowitz, O. Penrose, J. Amar, Scaling functions, self-similarity, and the morphology of phase-separating systems, Phys. Rev. B 44 (1991) 4794–4811. doi:10.1103/PhysRevB.44.4794.
URL http://link.aps.org/doi/10.1103/PhysRevB.44.4794

[36] T. Rogers, R. Desai, Numerical study of late-stage coarsening for off-critical quenches in the cahn-hilliard equation of phase separation, Phys. Rev. B 39 (0) (1989) 11956–11964. doi:10.1103/PhysRevB.39.11956.
URL http://link.aps.org/doi/10.1103/PhysRevB.39.11956

[37] H. Alt, Linear Functional Analysis, Springer, 2016.

[38] P. J. Flory, Thermodynamics of high polymer solutions, J. Phys. Chem. 10 (1942) 51–61. doi:10.1063/1.1723621.

[39] C. Wylock, M. Pradas, B. Haut, P. Colinet, S. Kalliadasis, Disorder-induced hysteresis and nonlocality of contact line motion in chemically heterogeneous microchannels, Physics of Fluids 24 (3) (2012) 32108. doi:10.1063/1.3696860.
URL http://link.aip.org/link/PHFLE6/v24/i3/p032108/s1&Agg=doi

[40] D. Boda, D. Gillespie, Steady-state electrodiffusion from the nernst-planck equation coupled to local equilibrium monte carlo simulations, J. Chem. Theory Comput. 8 (2012) 824–829.

[41] S. de Groot, P. Mazur, Non-equilibrium Thermodynamics, North-Holland, 1969.

[42] I. Kosinska, I. Goychuk, M. Kostur, G. Schmid, P. Hänggi, Rectification in synthetic conical nanopores: A one-dimensional poisson-nernst-planck model, Phys. Rev. E 77 (2008) 031131.

[43] P. Malgaretti, I. Pagonabarraga, M. Rubi, Entropic transport in confined media: a challenge for computational studies in biological and soft-matter systems, Frontiers in Physics 1 (21). doi:10.3389/fphy.2013.00021.
URL http://www.frontiersin.org/computational_physics/10.3389/fphy.2013.00021/abstract

[44] R. Kubo, The fluctuation-dissipation theorem, Rep. Prog. Phys. 29 (255).

[45] S. Brenner, L. Scott, The mathematical theory of finite element methods, Springer, 1994.

[46] J. Crank, P. Nicolson, A practical method for numerical evaluation of solutions of partial differential equations of heat-conduction type, Proc. Cambrdidge Philos. Soc. 43 (1947) 50–67.

[47] G. Lord, C. Powell, T. Shardlow, An introduction to computational stochastic PDEs, CUP, 2014.

[48] G. A. Chechkin, A. L. Piatnitski, A. S. Shamaev, Homogenization: Methods and Applications, American Mathematical Society, 2007.

[49] V. Zhikov, Some estimates from homogenization theory, Doklady Mathematics 73 (1) (2006) 96–99. doi:10.1134/S1064562406010261.
URL http://dx.doi.org/10.1134/S1064562406010261

[50] T. Suslina, Operator error estimates in l_2 for homogenization of an elliptic dirichlet problem, Funct. Anal. Appl. 46 (3) (2012) 234–238.

[51] S. Pastukhova, The dirichlet problem for elliptic equations with multiscale coefficients. operator estimates for homogenization, Journal of Mathematical Sciences 193 (2) (2013) 283–300. doi:10.1007/s10958-013-1453-z.
URL http://dx.doi.org/10.1007/s10958-013-1453-z

[52] N. D. Alikakos, P. W. Bates, X. Chen, Convergence of the Cahn-Hilliard equation to the Hele-Shaw model, Arch. Rational Mech. Anal. 128 (1994) 165–205.

[53] B. Kehlet, mshr is the mesh generation component of fenics.
URL https://bitbucket.org/fenics-project/mshr

[54] M. S. Alnæs, J. Blechta, J. Hake, A. Johansson, B. Kehlet, A. Logg, C. Richardson, J. Ring, M. E. Rognes, G. N. Wells, The fenics project version 1.5, Archive of Numerical Software 3 (100). doi:10.11588/ans.2015.100.20553.

[55] O. A. Oleĭnik, A. S. Shamaev, G. A. Yosifian, Mathematical problems in elasticity and homogenization, Vol. 26 of Studies in Mathematics and its Applications, North-Holland Publishing Co., Amsterdam, 1992.

[56] A.-L. Barabási, H. Stanley, Fractal Concepts in Surface Growth, Cambridge University Press, 1995.

[57] A. Novick-Cohen, The {C}ahn-{H}illiard equation, Vol. 4 of Handb. Differ. Equ., Elsevier/North-Holland, Amsterdam, 2008, pp. 201–228. doi:10.1016/S1874-5717(08)00004-2.
URL http://dx.doi.org/10.1016/S1874-5717(08)00004-2

[58] M. Schmuck, First error bounds for the porous media approximation of the Poisson-Nernst-Planck equations, Z. Angew. Math. Mech. 92 (4) (2012) 304–319.